



Polytechnic University of Timisoara



FACULTY OF MECHANICS

**Microstructure and cavitation erosion resistance of
weld-deposited layers on Duplex stainless steels**

- ABSTRACT -

Author:

Eng. Daniel Paul MUTAȘCU

Scientific leaders:

Prof. univ. dr. ing. Ion MITELEA

Prof. univ. dr. ing. Ilare BORDEAȘU

Timișoara, 2024

Content

(extras)

Introduction

Chapter 1 Current state of research

1.1 Introduction

1.2 Microstructure and properties of Duplex stainless steels

1.3 Mechanism of cavitation degradation

1.3.1 Mechanisms of cavitational erosion breakage

1.3.1.1 Influence of incubation period and strain rate

1.3.1.2 Influence of crystallization structure

1.3.1.3 Mechanism of fatigue breakdown

1.3.2 Observations in the Hydraulic Machines Laboratory in Timișoara

1.3.3 Manifestation of the cavitative damage mechanism as a function of the hydrodynamics of cavitation

1.3.3.1 Naval propeller

1.3.3.2 Hydraulic turbine rotors

1.3.3.3 Centrifugal pump rotor

1.4 Surface hardening techniques to improve cavitation resistance

1.4.1 Volumetric heat treatments and cavitation erosion resistance

1.4.2 Cavitation resistance of surfaces hardened by nitriding treatments

1.4.2.1 Gas nitriding

1.4.2.2 Laser beam nitriding

1.5 Objectives of the doctoral thesis

Chapter 2 Cavitation erosion of "Stellite 21" alloy layers deposited by TIG welding on the surface of Duplex stainless steels

2.1 Introduction

2.2 Particularities of the deposition process by pulsed TIG welding

2.2.1 TIG welding process basics

2.2.2 Pulsed TIG welding deposition process parameters

2.3 Microscopic investigations on the layer-substrate system

2.4 Dilution assessment. X-ray energy dispersive and macrographic analysis

2.5 Hardness tests

2.6 X-ray diffraction analysis

2.7 Cavitation resistance of Stellite 21 deposited layers

2.7.1 Experimental procedure

2.7.2 Cavitation curves

2.8 Conclusions

Chapter 3 Cavitation resistance of Corodur 65 alloy layers deposited by TIG welding on Duplex stainless steels

3.1 Introduction

3.2 Experimental procedure

3.3 Evaluation of experimental data

3.3.1 Chemical heterogeneities and degree of dilution

3.3.2 Microstructure of the layer-substrate system

3.3.3 X-ray diffraction analysis

3.3.4 Hardness measurements

3.3.5 Cavitation test results

3.3.6 Macrographic examinations of cavitation tested surfaces

3.3.7 Cavity surface roughness measurements

3.3.8 Topography of surfaces eroded by cavitation

3.4 Conclusions

Chapter 4 Structural characteristics and cavitation resistance of weld-deposited austenitic manganese-manganese alloy layers on Duplex stainless steels

4.1 Introduction

4.2 Materials, experimental procedure

4.3 Evaluation of experimental results

4.3.1 Macrographic examinations

4.3.2 Micrographic examinations

4.4 EDX analysis. Degree of dilution

4.5 X-ray diffraction

4.6 Hardness tests

- 4.6 Evaluation of cavitation tests
- 4.8 Cavity surface topography
- 4.9 Conclusions

Chapter 5 Final conclusions and original contributions. Future research directions

List of publications resulting from doctoral research, published or accepted for publication, under UPT affiliation

BIBLIOGRAPHY

Chapter 1 Current state of research

Cavitation erosion is the most harmful effect of cavitation, which occurs in the operation of hydraulic machinery and equipment, due to the destruction of the solid materials of which the boundaries that come into contact with the liquid are made. This phenomenon was first identified in 1848 with the testing of the first modern passenger ship, built of metal and propelled by a steam engine driving a steel naval propeller, built by Great Britain, designed by Isambard Kingdom Brunel and launched in 1843 [14]. In 1875, the Italian Bartellor records cavitation erosion on the propellers of the ships Mauritania and Luisitania [14]. The negative effects on the performance of a ship's propeller were only identified in 1893 by Parsons, who built the first cavitation tunnel [5].

With the passage of time, it has been found that cavitation-specific damage occurs in all equipment and installations working with liquids (hydraulic turbines and pumps, control and monitoring devices in hydraulic drive systems, valves, fittings and pumps of water supply and irrigation networks, etc.), where there are significant pressure variations, with a drop below the vaporization pressure and a sudden increase. For this reason, many parts that operate under cavitation conditions are made of materials that have physico-mechanical properties and microstructures that can withstand the fatigue stresses produced by microjet impacts and shock waves generated by the hydrodynamics of cavitation. Research carried out on hydraulic machine rotors and ship propellers [1],[4],[5], shows that stainless steels have good resistance to cavitation erosion, which can be improved by various heat treatments or surface hardening technologies. Of these, those with a martensitic structure have a somewhat higher strength. However, the difficulty of machining them has led scientists to look for ways of using austenite or combined steels, such as duplex (austenite-ferrite)

steels [18],[22]. This is why, in many cases, classic austenitic and Mo-containing austenitic stainless steels can be successfully replaced by austenitic-ferritic (duplex) steels. These alternative materials offer excellent corrosion resistance, higher mechanical properties, shock bending toughness down to -50 0C [20],[23], leading to reduced manufacturing costs. Thanks to these advantages, today Duplex stainless steels are increasingly used in the manufacture of parts subject to intense cavitation erosion (hydraulic machine rotors, naval propellers, control, distribution and regulating apparatus in hydraulic drive systems) [14]. In order to increase the service life of such equipment, the Cavitation Laboratory of the Polytechnic University of Timisoara has been carrying out research for over 80 years on various grades of steels subjected to the latest techniques for improving the characteristics that increase resistance to cavitation erosion [7], [8], [11], [12], [16], [24], [25].

Duplex stainless steels, in steady state, according to [9], [21], [22], [23], [27] have a ferritic-austenitic or austenite-ferritic structure (about 50% ferrite and 50% austenite) and are characterized by:

- corrosion stability under stress in aqueous fluids containing chloride ions and excellent point corrosion stability;
- high values of mechanical strength characteristics (yield strength and breaking strength);
- superior properties to classical austenitic stainless steels (X5CrNiNi18-10 and X2CrNiMoMo17-12-2) [2], [10];
- Ni content (expensive element), lower than that of austenitic stainless steels, which economically justifies its use in parts working in cavitation currents.

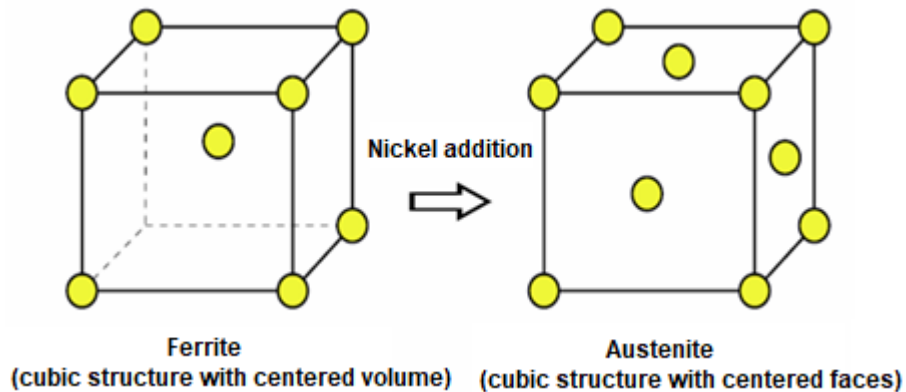


Figure 1.1 Crystal lattice type modification by nickel alloying

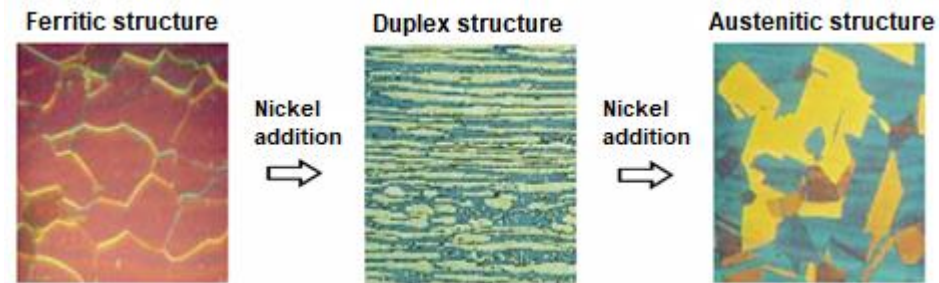


Figure 1.2 Microscopic structure modification by nickel alloying

The proportion of the two phases (austenite (A) and ferrite (F)), can be modified within broad limits, depending on:

- content in alloying elements;
- heating temperature for dissolving the intermetallic phases.

At the same time, the application of heat treatments causes the following phenomena with consequences on the microstructure change [23]:

- precipitation of M₂₃C₆-type carbides and Cr₂N-type nitrides on the interface of ferrite - austenite grains, without consequences on intercrystalline corrosion;
- slight precipitation of σ phase (from the ferrite) during heating;
- hardening by annealing at temperatures between 400 and 900°C.

In many cases, austenitic Mo-containing austenitic stainless steels can be successfully replaced by austenitic-ferritic (duplex) steels [23].

Figure 1.3 a,b and Figure 1.4 a,b show a Kaplan turbine rotor and a Francis turbine rotor, respectively, both before and after degradation by cavitation erosion [14]. The different and much more pronounced mode of destruction is observed for the Francis turbine rotor.



a)

b)

Figure 1.3 Kaplan stainless steel turbine rotor [14]:

a - turbine rotor before degradation by cavitation erosion;

b - rotor blade after cavitation erosion degradation.



a)

b)

Figure 1.4 Francis turbine rotor made of stainless steel [4]:

a – turbine rotor before degradation by cavitation erosion;

b – rotor blade after cavitation erosion degradation.

The objectives of the doctoral thesis are:

- investigating the behavior and vibrational cavitation resistance of weld deposited layers on duplex stainless steel X2CrNiMoN22-5-3;
- to investigate the degradation mechanism of surface layers under vibrational cavitation stresses;
- investigating the morphology and the macro- and microstructural characterization of surfaces subjected to cavitation erosion with the study of the mechanism of crack and rupture generation and propagation;

The novelty of the doctoral thesis:

The novelty of the doctoral thesis consists in finding a correlation between the structural state of the material of the layer deposited by welding on samples of duplex stainless steel X2CrNiMoN22-5-3 and the parameters of degradation by cavitation erosion ("1/MDER" "MDE", "Rz") and optimizing the technological welding process in order to increase the service life of parts working in such hydrodynamic conditions.

Chapter 2 Cavitation erosion of "Stellite 21" alloy layers deposited by TIG welding on the surface of Duplex stainless steels

This chapter analyzes the process parameters of pulse TIG deposition of lower carbon "Stellite 21" alloys on Duplex stainless steel substrates, X2CrNiMoMoN22-5-3. Optimized process parameters are presented together with an analysis of the hardness and structure of the deposited layer. The role of layers of these "Stellite 21" alloys, deposited by the TIG welding process on Duplex stainless steels to reduce surface degradation of parts subject to cavitation erosion, is also investigated.

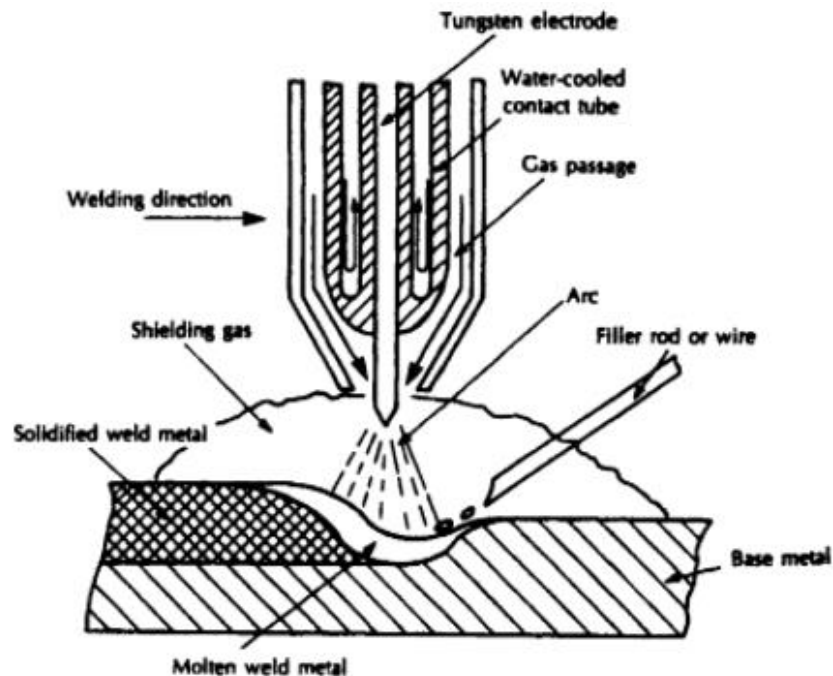
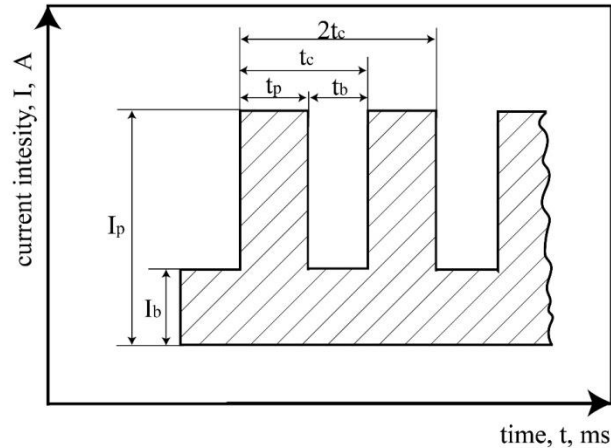


Figure 2.1 TIG welding charging process

In manual operation, the alloys selected for hardening are delivered in the form of metal rods and are melted and flowed onto the substrate to form the deposited layer. In automated operation, this process usually requires an alloy feeder and part handling devices.



- I – current** **t – time**
- I_p – pulse current** **I_b – basic current**
- t_p – pulse time** **t_b – basic time**
- t_c – cycle time** **f – pulse frequency ($f = \frac{1}{t_c}$)**
- $t_a = \frac{t_p}{t_p + t_b} \cdot 100$ [%] (active pulse time)**

Figure 2.2 Pulsed current TIG welding process parameters

The material subject of the experimental research carried out is the Duplex 2205 stainless steel brand, symbolized X2CrNiMoN22-5-3 according to the European standard EN 10088 and UNS S31803 according to ASTM A276. It was subjected to solution heat treatment at 1060 °C with quenching in water. The typical microstructure of this heat-treated steel, as assessed by quantitative metallographic determinations using a Fischer feritscope, is composed of ca. 48 % ferrite and 52 % austenite.

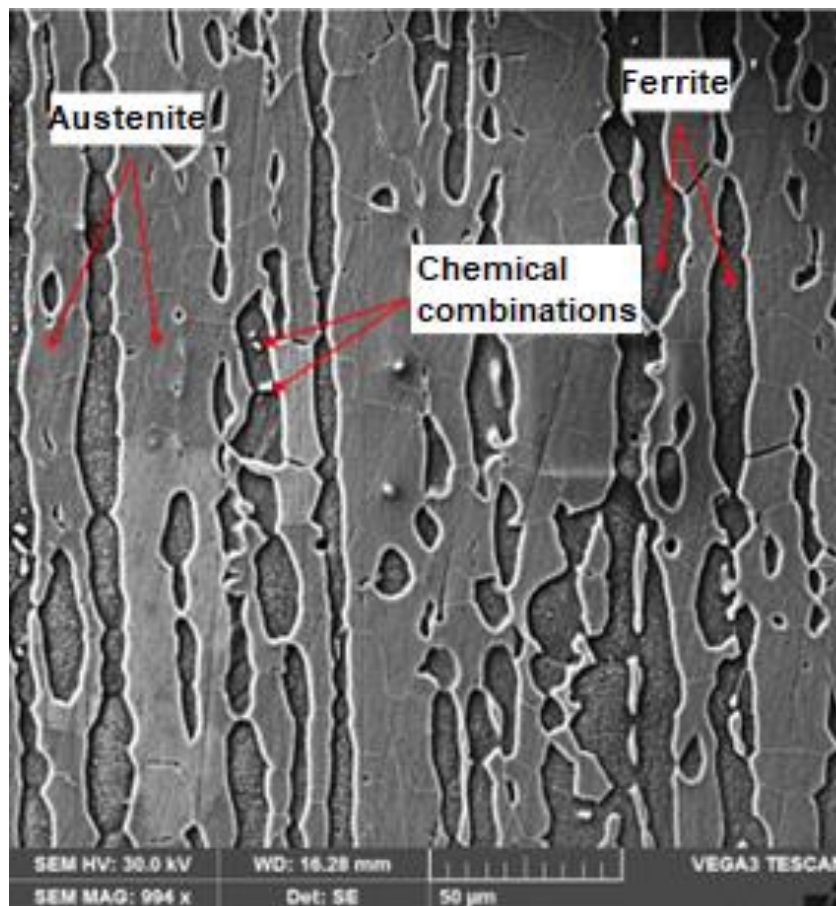


Figure 2.3 Duplex stainless steel substrate microstructure - SEM x 994

Chemical composition of the steel used as substrate:

C, %	Si, %	Mn, %	P, %	S, %	Cr, %	Ni, %	Mo, %	N, %
0,021	0,79	0,82	0,019	0,012	22,34	5,61	3,1	0,14

The microstructure of the deposited layer of Stellite 21 alloy is shown in figure 2.4. As demonstrated in other research works [32], [59], it consists of a Co-rich matrix with a dendritic appearance in which particles of carbide-like chemical combinations are distributed. Both Cr as the main alloying element and Mo, are elements that react with C to form carbides distributed in the interdendritic zones and on the boundaries of crystalline grains. They have size and distribution dependent on processing conditions.

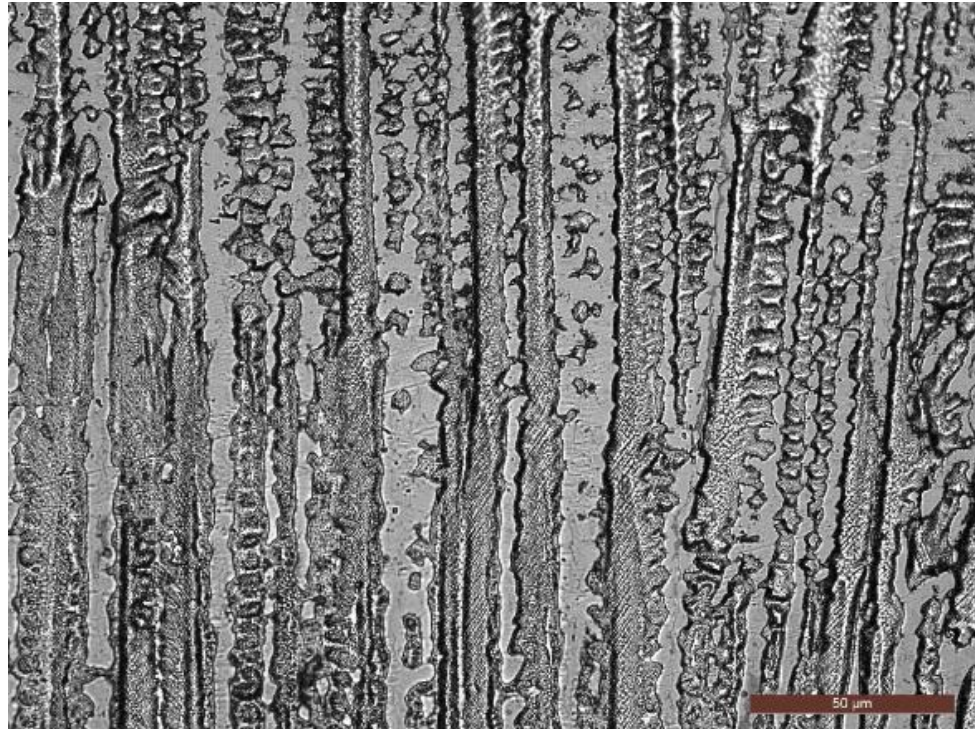


Figure 2.4 Microstructure of the outer zone of the deposited layer - x 300

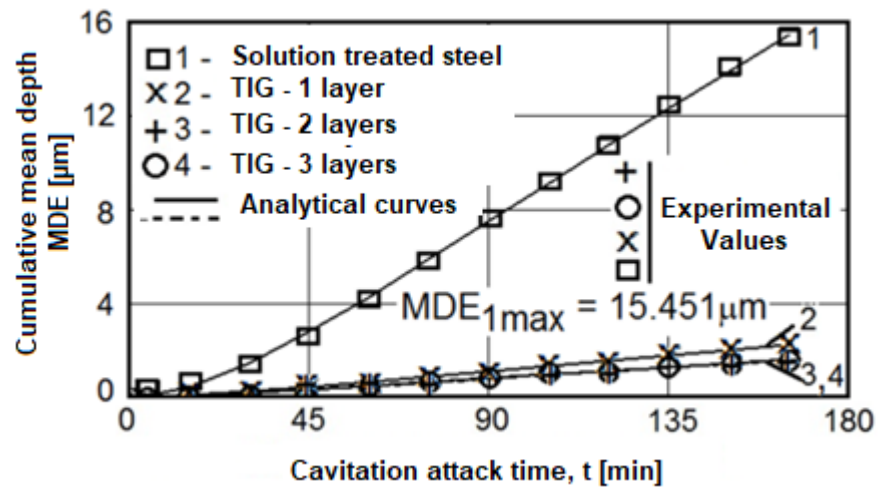


Figure 2.5 Evolution of erosion penetration depth with duration of cavitation attack

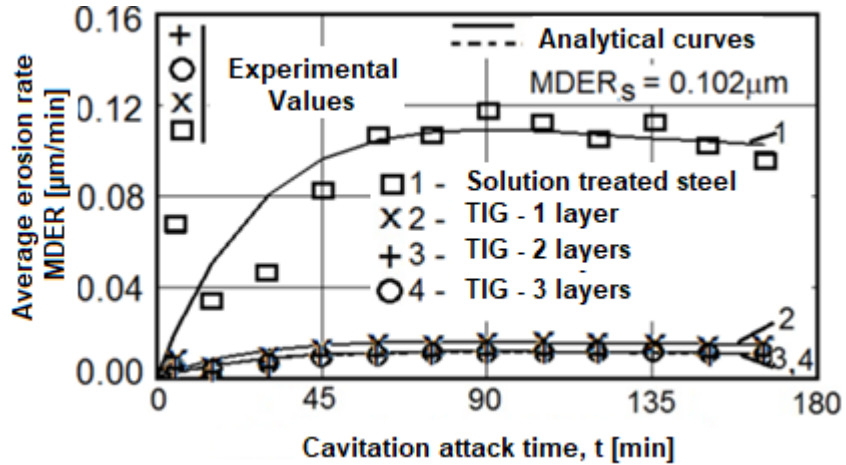


Figure 2.6 Variation of erosion rate with duration of cavitation attack

The analysis of the data in Figures 2.5 and 2.6 reveals the following observations:

- after 165 min. of cavitation attack, the mass loss of Duplex stainless steel is approx. 24 mg and the cavitation erosion rate is ca. 0.16 mg/min.;
- compared to the base material, TIG welded layers show a decrease in mass loss by (7÷10) times and in erosion rate by (7÷11) times;
- independent of the number of deposited TIG layers, the resistance to cavitation erosion of "Stelite 21" alloy is excellent.

Scanning electron microscope examination of cross-sections through cavity surfaces for 165 min (figure 2.7) allows the following observations:

- the onset of cavitation attack is initiated at the phase boundaries, followed by the removal of carbide particles, and then attack of the cobalt-based solid solution matrix;
- the low values of linear energy characteristic of the pulsed TIG process lead to microstructure finishing. The smaller the size of the grains, the larger the areas of the grain boundaries between them and the more pronounced will be the effect of blocking cavitation degradation;
- a mechanical and phasic hardening of the surface layer, with a thickness of 280...410 μm, caused by the mechanical action of the imploding of cavitation bubbles, respectively by the induction of a martensitic transformation.

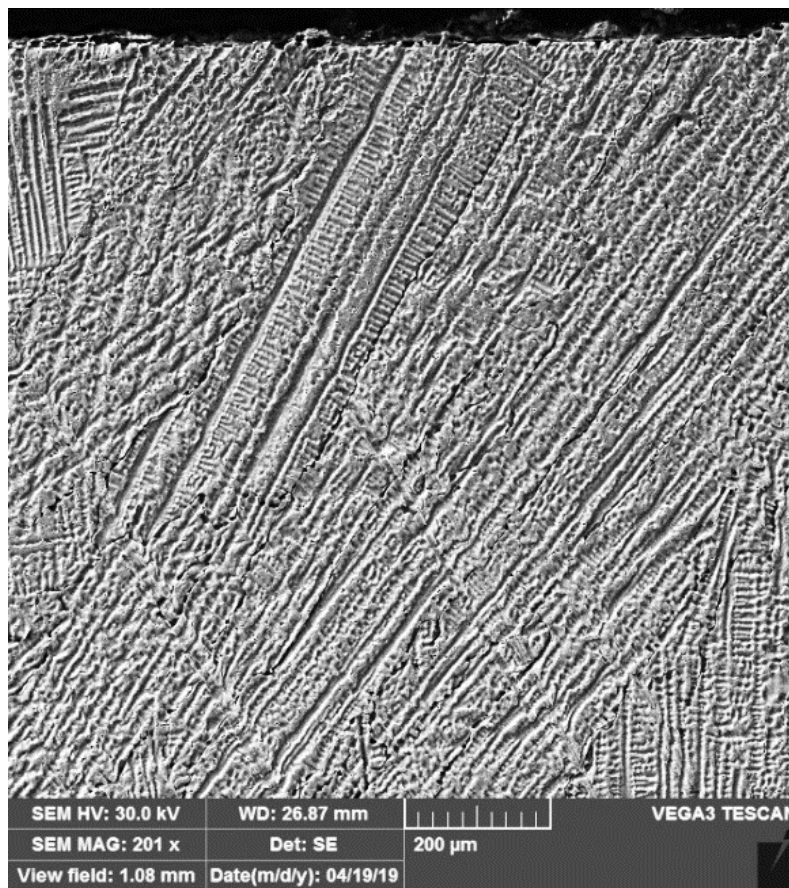


Figure 2.7 SEM image of a cross-section through the cavitation test samples

Chapter 3 Cavitation resistance of Corodur 65 alloy layers deposited by TIG welding on Duplex stainless steels

This chapter analyzes the process parameters of TIG deposition of Corodur 65 (EN 14700 DIN 8555) electrode wire (EN 14700) on Duplex stainless steel substrates, X2CrNiMoN22-5-3 with potential applications in the refurbishment of mechanical systems working under mechanical wear and cavitation erosion conditions. The optimized process parameters are presented together with an analysis of the diffusion of alloying elements from the base metal into the deposited metal, the hardness gradient, the macro- and microstructure of the layer-substrate system and the resistance performance to cavitation erosion.

The addition metal selected for the experiments was Corodur 65, (Corthal 65), - DIN EN 14700, which has the following chemical composition: C = 5.08 %, Si = 0.94 %, Mn = 0.42 %, Cr = 21.1 %, Mo = 6.94 %, Nb = 6.72 %, V = 1.02 %, W = 1.88 %, Fe = Rest.

This alloy was chosen because it has special characteristics in terms of high resistance to abrasive wear, due to its chemical composition that combines high C content with Cr, Mo, Nb,

W and V, while maintaining a lower Fe content. The base metal used was stainless steel X2CrNiMoN22-5-3 (AISI 2205).

The dosing of the linear energy introduced into the workpiece is achieved by adjusting the technological parameters I_p , I_b , t_p , t_b and the frequency f . At the same value of the average welding current, the seam penetration is higher than in classical TIG welding and the linear energy is lower, which leads to a reduction of the welding stresses and strains. As general recommendations, the pulse current has values 1.5 - 2 times higher than the classical constant current

$$I_p = 1,8 I_{ref.}$$

$$I_b = I_p/3 \text{ (rule of thirds)}$$

$$t_p = 0,2...0,3 \text{ s}$$

$$t_b = 2 \times t_p$$

In this case you get:

$$I_{ref.} = (I_p \times t_p + I_b \times t_b)/(t_p + t_b)$$

Example:

$$\text{for: } I_{ref.} = 50 \text{ A,}$$

it follows:

$$I_p = 90 \text{ A}$$

$$I_b = I_p/3 = 30 \text{ A}$$

$$t_p = 0,3 \text{ s}$$

$$t_b = 2 \times t_p = 0,6 \text{ s}$$

$$I_m = I_{ref.} = (I_p \times t_p + I_b \times t_b) / (t_p + t_b) = (90 \times 0,3 + 30 \times 0,6) / (0,3 + 0,6) = (27 + 18) / 0,9 = 45 / 0,9 = 50 \text{ A}$$

For chemical and metallographic analysis, the samples were cross-sectioned and then prepared by conventional metallographic techniques; after cutting, they were sanded with silicon carbide abrasive paper and polished with diamond paste, and finally chemically attacked with V2A reagent.

The dilution phenomenon is caused by the difference between the melting points of the base metal and the hard coating alloy. The process of hard loading of a substrate is accompanied

by a penetration of its component elements into the deposited metal, affecting to some extent the properties of the hard coating alloy. Consequently, the properties of the alloy are diluted down to a certain region at the interface known as the dilution region. The evaluation of the degree of dilution was based on the chemical composition of the three distinct regions (base metal, deposited metal and additive metal) using X-ray energy dispersive analysis. The calculation relation is [17]:

$$Gd = (F_{ewm} - F_{efm}) / (F_{ebm} + F_{efm}) \times 100 = (65.02 - 55.90) / (67.27 + 55.90) \times 100 = 7.4 \%$$

where F_{ewm} , F_{efm} and F_{ebm} are the iron contents in weight percent of weld metal, filler metal and parent metal.

Microscopic analysis provides knowledge to assess the quality of the deposited layers. The microstructural examinations were conducted on a Leica DM 2700 M optical microscope and a Bruker TESCAN VEGA 3 LMU scanning electron microscope equipped with a Bruker TESCAN VEGA 3 LMU energy dispersive X-ray (EDX) analysis system.

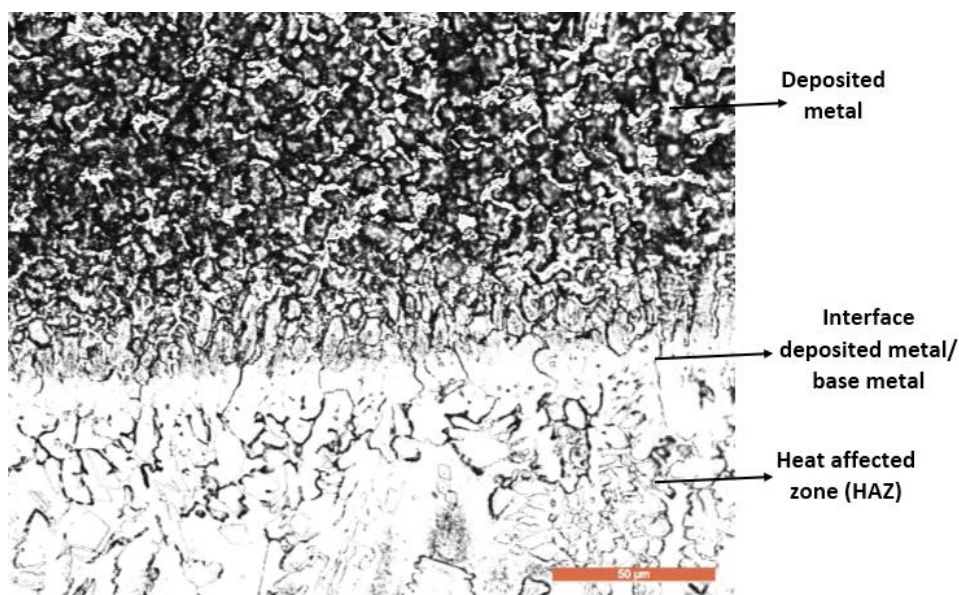


Figure. 3.1 Optical microscopy, x 500 - microstructure of the interface between the deposited metal and the base metal

Scanning electron microscope investigations reveal that secondary phases are precipitated in both intercellular and interdendritic regions. The cellular and cell-dendritic structures are located at the bottom of the fusion zone, just behind the line of its interface with the base metal.

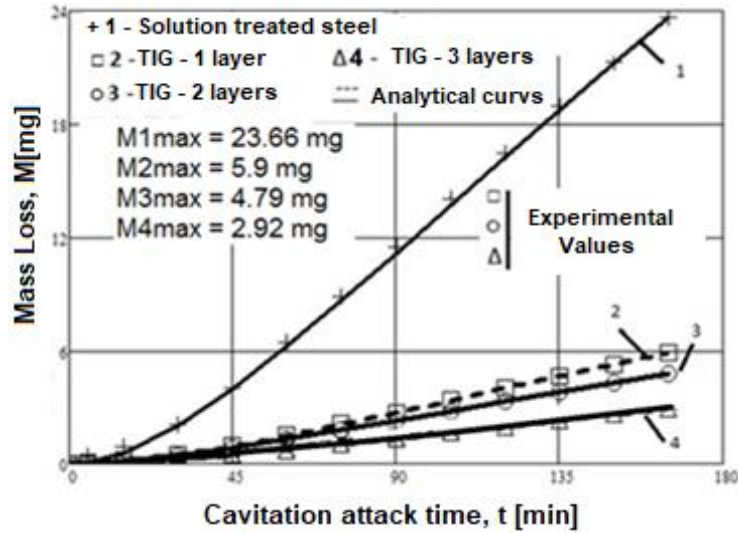


Figure 3.2 Evolution of mass loss with duration of cavitation attack

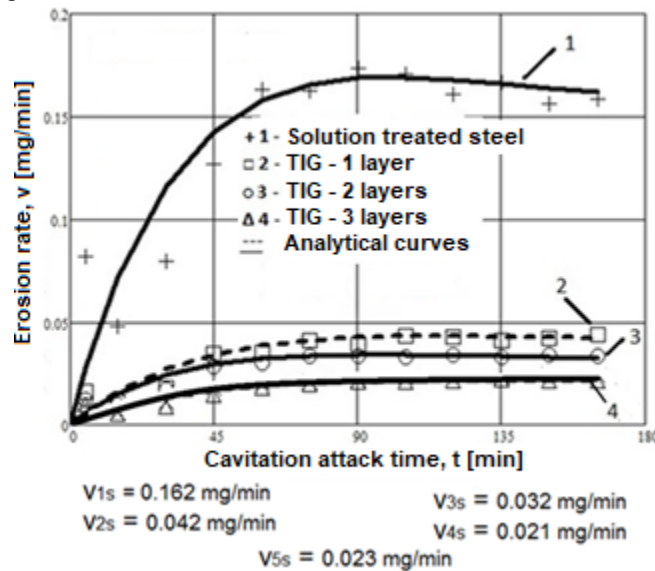


Figure 3.3 Variation of erosion rate with duration of cavitation attack

The findings from the diagrams in figures 3.2 and 3.3 are:

- 1- the evolution of the mass loss curves (figure 3.2), with linear variation starting from minute 75, and of the erosion rates, with a tendency to stabilize at the maximum value after the same exposure time, suggest, as specified in [13], [19], [26] that the layers resistance is high, specific for surfaces with high hardness, relatively fine structure and homogeneous dispersion of the mechanical properties in the volume of the deposited layer;
- 2- the dispersion of the experimental values of the erosion velocities with respect to the averaging curve (figure 3.3) is the expression of a fine-grained structure [15], which leads to an increased resistance to cavitation erosion;
- 3- comparison with the substrate material, the curves marked with 1, show that:

- a. the increase in strength expressed by the total mass value (M_{\max} , after 165 minutes) varies from 4.01 to 8.1 times, depending on the number of layers;
 - b. the increase in strength, as a function of the number of layers deposited by TIG welding, expressed by the value towards which the erosion rate tends to stabilize (v_s) after 165 minutes of cavitation attack, varies from 3.9 to 7.7 times;
- 4- Increasing the number of layers deposited by TIG welding leads to increased cavitation resistance. Surfaces with 3 and 4 layers have approximately identical behavior and strengths, higher by (80...100)%, compared to the surface with one layer deposited and higher by (39...50)% compared to the surface with two layers.
- 5- The fact that between 3- and 4-layer surfaces the differences in behavior and resistance to cavitation erosion is insignificant shows that any increase in the number of layers above 3 is uneconomical.

In figure 3.4 show the SEM image of the surface of the 3-layers deposited sample, which was tested by cavitation erosion for 165 min. In this situation, carbide particles were preferentially removed as a result of initial deformation and crack generation at the particle - austenitic matrix interface. As a consequence, this plastic deformation causes the initiation and propagation of fatigue micro-cracks, which ultimately lead to fatigue failure and material erosion.

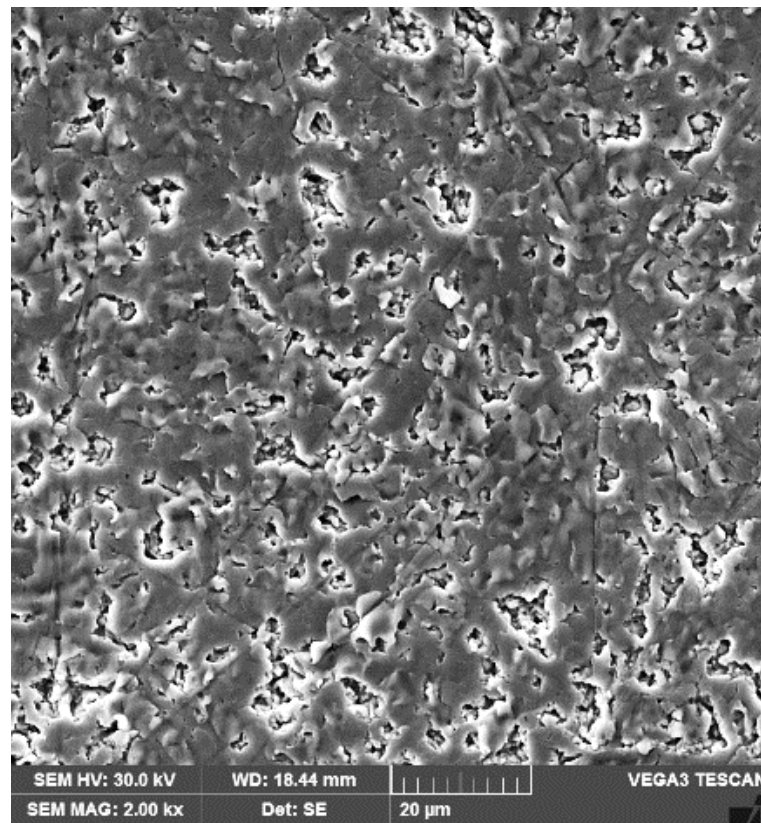


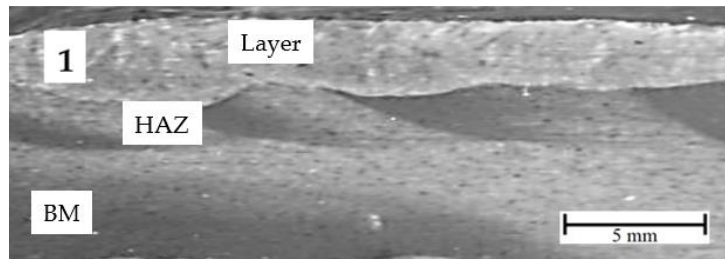
Figure 3.4 SEM images of cavitation degraded surfaces - 3 deposited layers

Chapter 4 Structural characteristics and cavitation resistance of weld-deposited austenitic manganese-manganese alloy layers on Duplex stainless steels

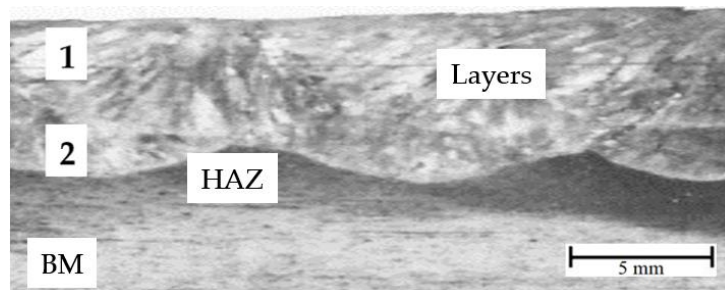
The base material used as substrate was Duplex 2205 stainless steel, symbolized X2CrNiMoN22N22-5-3 according to the European standard EN 10088 and UNS S31803 according to ASTM A276. Prior to the hardfacing process it was subjected to solution quenching heat treatment at a temperature of 1060 °C with quenching in water.

The selected additive material was CITOMANGAN electrode with basic coating of manganese austenitic steel, symbolized DIN 8555: ~E 7 - UM - 200 KP, respectively EN 14700: E Fe 9 which is recommended for wear resistant layer deposition under high impact and shock conditions. The guaranteed chemical composition of the deposited metal is as follows: 0.60 % C, 15 % Mn, 4.5 % Cr, 4.8 % Ni, rest Fe.

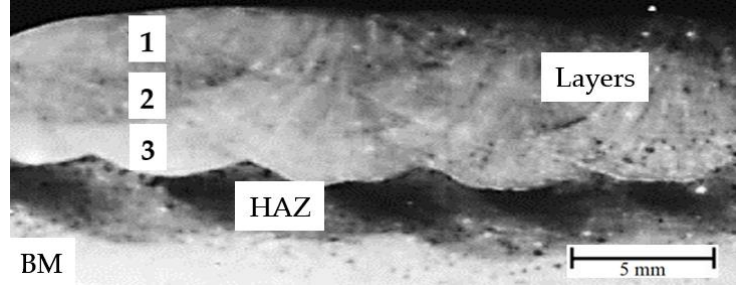
Figure 4.1 shows examples of macrographic images of samples loaded with one, two and three layers. These images highlight a proper geometry of the deposited metal zone, and the absence of material continuity defects. Since austenitic steel does not exhibit polymorphic transformation, no grain refinement is possible in the thermally influenced zone (HAZ), and the large grains resulting from each pass appear to impede each other in growth.



a)



b)



c)

Figure 4.1 Macro images of the layer-substrate system: a) - 1 layer deposited; b) - 2 layers deposited; c) - 3 layers deposited

In order to follow and analyze the behavior of metallic alloys under cavitation attack, specific diagrams are constructed containing the experimental values of the cumulative eroded mass M_i and the average erosion penetration velocity v_i , as well as the variations of the averaging curves $M(t)$ and $v(t)$ of these values.

- for the experimental value of cumulative eroded mass:

$$M_i = \sum_{i=1}^{i=13} \Delta m_i \quad [\text{mg}] \quad (1)$$

- for the analytical averaging curve of the experimental values of the cumulated eroded mass: [3], [6].

$$M(t) = A \cdot t \cdot (1 - e^{-B \cdot t}) \quad (2)$$

- for the experimental value of the mean erosion rate for the intermediate period:

$$v_i = \Delta m_i / \Delta t_i \quad [\text{mg/min}] \quad (3)$$

- for the analytical curve averaging the experimental values obtained for the mean erosion rates [3], [6]:

$$v(t) = A \cdot (1 - e^{-B \cdot t}) + A \cdot B \cdot t \cdot e^{-B \cdot t} \quad (4)$$

where:

for $i = 1$, $\Delta t_i = 0$, $M_i = 0$

i - is the number of intermediate test period;

Δm_i - is the mass of material lost by erosion in period i , in grams;

Δt_i – duration of the intermediate 'i' period of cavitation (5, 10 and 15) in minutes;

A - is the scale parameter, statistically established on the basis of the experimental values, used to construct their approximation / averaging curve, provided that their deviations from it are minimal;

B - is the shape parameter of the curve, statistically determined from experimental values.

The values of the parameters A and B were set in the Matchad program, following a model built in the Cavitation Erosion Research Laboratory in Timișoara [3], [6].

The relations used to determine the mean standard deviation σ and the boundaries $S(t)$ and $I(t)$, as used in the literature [6], adapted to the experimental data in the diagrams, have the forms:

- for the mean standard deviation:

$$\sigma = \left[\frac{\sum_{i=0}^{13} (M_i - M(t)_i)^2}{n - 1} \right]^{\frac{1}{2}}, n = 13 \tag{5}$$

- for tolerance range 99%:

$$S99(t) = M(t) + 1 \cdot \sigma ; I99(t) = M(t) - 1 \cdot \sigma \tag{6}$$

- for Tolerance range 90%:

$$S90(t) = M(t) + 10 \cdot \sigma ; I90(t) = M(t) - 10 \cdot \sigma \tag{7}$$

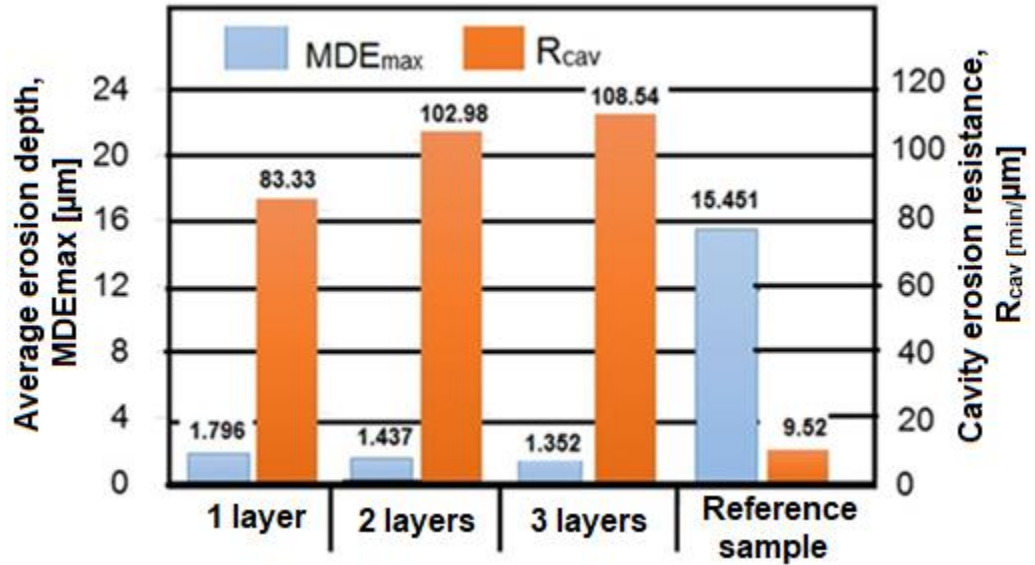


Figure 4.2 Histogram comparing cavitation erosion resistance

It should be noted that the parameters MDE_{max} and R_{cav} , indicated by ASTM G32-2016 [28] are determined with the relations used in our laboratory custom [3], [6]:

$$MDE_{max} = \frac{4 \cdot M_{max}}{\rho \cdot \pi \cdot d_p^2} \quad [\mu m] \tag{8}$$

$$R_{\text{cav}} = \frac{\rho \cdot \pi \cdot d_p^2}{4 \cdot v_s} \text{ [min/ } \mu\text{m]} \quad (9)$$

where:

M_{max} - cumulated mass (figure 4.14);

ρ - steel density, (7810 kg/m³);

d_p – diameter of the sample surface subjected to cavitation attack ($d_p = 15,8$ mm);

v_s – the value of the speed towards which the curve $v(t)$ tends asymptotically (final value figure 4.15).

The histogram presented in figure 4.2 shows:

- by the deposition of 2-3 layers of austenitic manganese austenitic alloy, the resistance to cavitation erosion is clearly superior to the structure of Duplex stainless steel, resulting from the solution hardening heat treatment (control, reference sample).
- according to the values of the two parameters, the resistance of the deposited layers to cavitation microjet stresses increases compared to that of the steel structure heat-treated by solution quenching from 8.6 times to 11.4 times, regardless of the parameter to which we refer MDE_{max} or R_{cav} ;
- of the three regimes, the highest strength is obtained for regimes 2 (with two layers) and 3 (with three layers); the difference between their strengths being insignificant (about 6 % after MDE_{max} and about 5.4 % after R_{cav} - practically within the accepted error margin for the mechanics of erosion produced by cavitation [3], [6];
- the increase in cavitation resistance achieved by the two- and three-layer deposited surfaces compared to that of the single-layer deposited surface is (23...30)%.

The process of hardfacing by welding is accompanied by a penetration of the component elements of the substrate material into the first layer of deposited metal. Therefore, the dilution of the deposited layer occurs as a result of mixing with the molten substrate, and affects its functional properties to some extent. It is good to know that dilution increases with increasing linear energy in welding. The degree of dilution was measured by chemical composition using energy dispersive X-ray (EDX) analysis (Figure 4.3). The calculated relationship is :

$$Gd = (F_{\text{ewm}} - F_{\text{efm}}) / (F_{\text{ebm}} + F_{\text{efm}}) \times 100 = (81.02 - 75.10) / (65.27 + 75.10) \times 100 = 4.2 \%$$

where:

Gd is the degree of dilution;

Fewm is the Fe content in the deposited layer, % mass;

Fefm is the Fe content in the admixture material, % mass;

Febm is the Fe content in the parent material, % by mass.

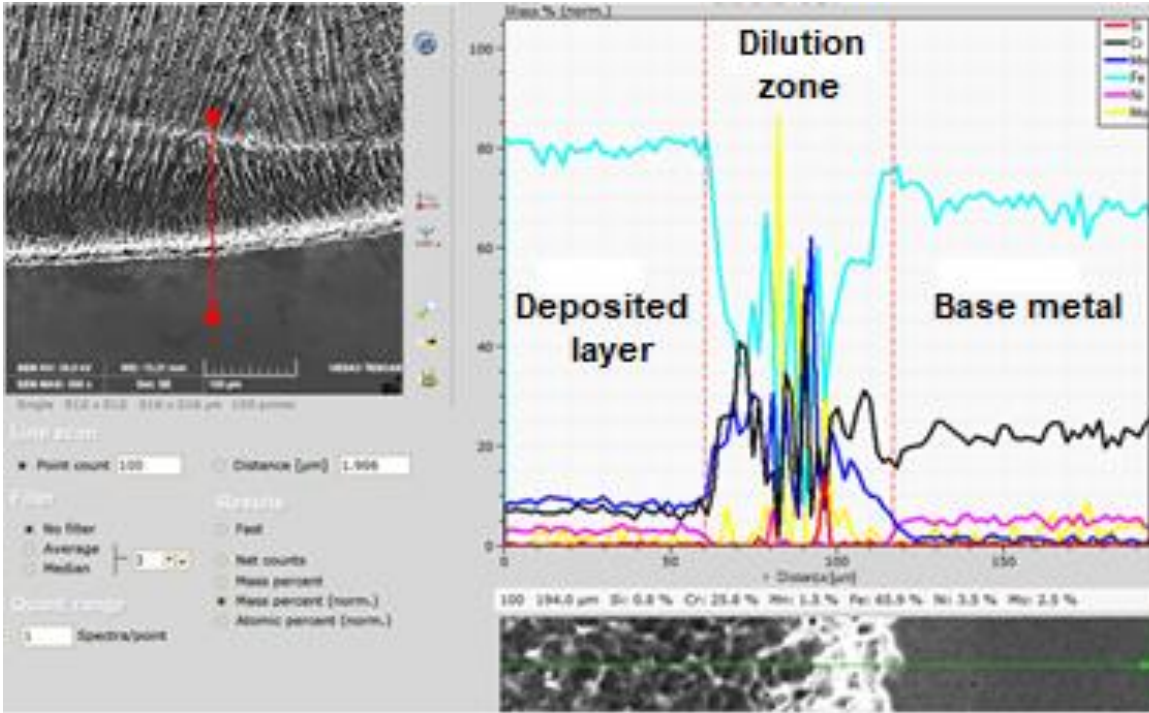


Figure 4.3 SEM image and alloying element concentration profiles on either side of the interface between the deposited metal and the base metal

Chapter 5 Final conclusions and original contributions. Future research directions

The doctoral thesis "Microstructure and resistance to cavitation erosion of weld-deposited layers on Duplex stainless steels" is part of the current trend in Materials Engineering and Mechanical Engineering research to find efficient solutions to improve this surface property by applying high-performance surface engineering technologies and to investigate the mechanism of surface degradation following the imploding of cavitation bubbles.

The main conclusions and original contributions of the paper can be summarized as follows:

1. The investigation of cavitation erosion is a critical problem driven by the multitude of factors that define the flow hydrodynamics and the structural state of the material.
2. Duplex stainless steels in solution hardening have a poor resistance to cavitation erosion compared to other stainless steels, which is attributed to the presence of ferrite in the microstructure and α/γ (ferrite/austenite) interfaces.
3. The deposition of 2 - 5 mm thick layers of Stellite 21" alloys by pulsed current TIG welding favors an increase in cavitation erosion resistance of 7 - 11 times, even in the first layer hardened by this process, proving its feasibility by:
 - precise dosing of the energy introduced into the material, which ensures a good layer-substrate metallurgical bond;
 - a low dilution of the additive material with the substrate material (approx. 5.9 - 6.1%) which is justified by the low heat input;
 - a shell microstructure consisting of a Co-based matrix and Cr carbides of the types Cr_3C_2 and Cr_7C_3 and Mo carbides;
 - a coating hardness of 358 - 401 HV5, which is significantly higher than that of the selected substrate of approximately 275 ± 15 HV5.
4. Investigation of the microstructural characteristics and resistance to cavitation erosion of Corodur 65 alloy layers deposited by pulsed-current TIG welding on the same reference material led to the following observations:
 - The process parameter that has the greatest influence on the linear energy and melting of the materials selected for the layer and substrate is the welding current.
 - The surface hardness of the deposited layers is extremely high, reaching values of approx. 810 HV5.
 - The experimentally established hardening process promotes precipitation reactions of finely dispersed complex carbides in a tenacious austenite matrix in the coating layer.
 - Precipitation of carbide phases occurs in both the intercellular and interdendritic regions of the fusion zone in close proximity to the base metal.

- The chemical composition profile, in a direction transverse to that of cell and dendritic growth, indicates an increase in Cr concentration and a decrease in Fe concentration in the intercellular region.

- Compared to the base metal, TIG welded Corodur 65 layers contribute to a 4.01 - 8.1 times reduction in mass loss and a 3.9 - 7.7 times reduction in erosion rate.

5. The pulsed-current electric arc hand-arc welding loading process, using austenitic manganese-manganese alloys with high sensitivity to mechanical strain hardening, offers opportunities for improving the resistance to cavitation erosion, mainly due to the following factors:

- The parameters set for the manual pulsed arc welding process ensure a reduction in the heat introduced into the material and an increase in the cooling rate, thus limiting the degree of dilution and the carbide phase precipitation phenomena;

- Following mechanical surface roughening, the hardness of the first deposited layer, affected by dilution, has values of 355 - 365 HV₅, while the hardness of the second and third deposited layers reaches values of 468 - 492 HV₅;

- The microstructure of the last layer deposited is austenitic with a cellular - dendritic character and with a low proportion of carbides so that a large part of the heat developed during welding is taken up by the water in which the largest mass of base material has been placed;

- The high mechanical work-hardenability of the austenitic manganese alloy, selected as additive material, justifies the significant improvement of the cavitation erosion resistance of Duplex stainless steel, considered as the base material;

6. Scanning electron microscope investigations have demonstrated that surfaces hardened by the welding techniques used with the selected filler materials and tested to cavitation erosion for 165 min. undergo uniform material degradation and less wear penetration compared to the substrate material.

7. The exponential evolutions on the first part, with the tendency of linearization on the second part of the averaging curves of the results $M(t)$ and of increase towards a maximum value, with

decrease towards the stabilization value, of the curves $v(t)$, confirm the hardening of the layer stressed by shock waves and cavitation microjets, as well as the shock damping effect created by the air/water penetrated into the caverns during the compression phase of the oscillatory mechanical system.

8. The statistical processing of the data obtained from the cavitation tests shows that in general the distribution of the experimental points with respect to the approximation curves is uniform for both penetration depth and erosion rate.

9. For all the experimental conditions used, the high accuracy of performing vibratory cavitation erosion tests and of processing the results is evidenced by the low mean standard deviation and high tolerance range values.

10. EDX analysis revealed chemical composition changes in the first and the last deposited layer compared to the reference material, helping to explain the microstructural characteristics of the deposited layers and the interface of the layer-substrate system.

11. X-ray diffraction revealed the nature of the microstructural phases formed in the deposited metal layers, which are responsible for the increase in hardness and hence in resistance to cavitation erosion.

Future research directions

1. Opportunities to improve the cavitation erosion resistance of Duplex stainless steels by applying high temperature gas nitriding (1050 - 1200 °C) followed by low temperature nitriding (500 - 550 °C) and vacuum carburizing thermochemical treatment.
2. To study the correlation between the influence magnitudes provided by fractal analysis and cavitation erosion test data.

Selective bibliography

1. Anton I.: Cavitația, vol. I, Editura Academiei RSR București, 1984;
2. Aribo S., Barker R., HU X., Neville A.: Erosion-corrosion behaviour of lean duplex stainless steels in 3,5% NaCl solution. *Wear*, vol. 302, 2013, pp. 1602 – 1608;

3. Bordeășu I., Pătrășcoiu C., Bădărău R., Sucitu L., Popoviciu M., Bălășoiu V. : New contributions in cavitation erosion curves modeling, FME Transactions Faculty of Mechanical Engineering, New Series, vol. 34, Nr.1/2006, YU ISSN 1451-2092, University of Belgrade, 2006, pp. 39-44;
4. Bordeășu I.,: Eroziunea cavitațională asupra materialelor utilizate în construcția mașinilor hidraulice și elicelor navale. Efecte de scară, Teză de doctorat, Timișoara, 1997;
5. Bordeășu I.: Eroziunea cavitațională a materialelor, Editura Politehnica, Timișoara, 2006;
6. Bordeasu, I.: Monografia Laboratorului de Cercetare a Eroziunii prin Cavitație al Universitatii Politehnica Timisoara, 1960-2020. Editura Politehnica, Timișoara, Romania, 2020;
7. Cojocaru V.: Cercetări privind creșterea duratei de viață a paletelor turbinelor hidraulice supuse la eroziune cavitațională, Teză de doctorat, Universitatea Eftimie Murgu din Reșița, 2013;
8. Coussement C.: Application industrielle de l'acier inoxydable duplex dans l'industrie pétrochimique - endommagement d'un serpentin de réacteur en duplex. Revue de la soudure, vol.2, 1994, pp.52-55;
9. Garcia R., Hammitt F. G., Nystrom R.E.: Correlation of cavitation damage with other material and fluid properties, Erosion by Cavitation or Impingement, ASTM, STP 408 Atlantic City, 1960;
10. Hrivnak I.: Duplex stainless steel and their welding, Zvaranie, nr. 3-4, 2002, pp.49-54;
11. Jurchela A.D.: Cercetări asupra eroziunii produse prin cavitație vibratorie la oțelurile inoxidabile cu conținut constant în crom și variabil de nichel, Teza de doctorat, Timișoara, 2012;
12. Karabenciov A.,: Cercetări asupra eroziunii produse prin cavitație vibratorie la oțelurile inoxidabile cu conținut constant în nichel și variabil de crom, Teza de doctorat, Timișoara, 2013;
13. Koseki S., Inoue K., Morito S., Ohba T., Usuki H.: Comparison of TiN-coated tools using CVD and PVD processes during continuous cutting of Ni-based superalloys. Surface and Coatings Technology, Vol. 283, 2015, pp. 353-363;
14. Lazăr, I: Tehnici de optimizare a rezistenței la eroziune prin cavitație a unor aliaje Cu-Zn și Cu-Sn, Teza de doctorat, Timișoara, 2020;

15. Madadi F., Ashrafizadeh F., Shamanian M.: Optimization of pulsed TIG cladding process of stellite alloy on carbon steel using RSM. *Journal of Alloys and Compounds*, Vol. 510, 2012, pp. 71 – 77;
16. Mânzână M.E.: Studii și cercetări experimentale privind modificările structurale produse prin cavitație-eroziune în diferite materiale metalice, Teza de doctorat, Bucuresti, 2012;
17. Messler R. W.: *Principles of Welding - Processes, Physics, Chemistry, and Metallurgy*. WILEY- VCH Verlag GmbH Weinheim, 2004, pp. 49 – 154;
18. Micu, L.M.: Comportarea la eroziune prin cavitație a oțelurilor inoxidabile duplex, Teza de doctorat, Timișoara, 2017;
19. Ming Q., Lim L.C, Chen Z.D.: Laser Cladding of nickel-based hardfacing alloys. *Surf Coating Technol*, vol.106, 1998, pp. 174-182;
20. Mitelea I., Budau V.: *Materiale și tratamente termice pentru structuri sudate*, Editura de Vest, 1992;
21. Mitelea I., Dimian E., Bordeășu I., Crăciunescu C.M.: Ultrasonic cavitation erosion of gas nitrided Ti-6Al-4V alloys, *Journal Ultrasonics Sonochemistry*, 21, 2014, pp.1544 – 1548;
22. Mitelea I.: 2009, *Materiale ingineresti*, Editura Politehnica, Timișoara, România;
23. Mitelea I.: *Știința materialelor*, vol.I, Editura Politehnica, Timișoara, 2009;
24. Popoviciu M., Bordeășu I.: Cavitation resistance evaluation for materials used in ship propellers and hydraulic turbine manufacturing, *Buletinul Științific și Tehnic al Universității Tehnice*, Timișoara, Vol 39, Nr.53, Fascicula 1-2, 1994;
25. Steller J.K.: International cavitation erosion test – summary of results, *ImechE Cavitation Conf.*, 1992, pp.95-102;
26. Thakur A., Gangopadhyay S.: Influence of tribological properties on the performance of uncoated, CVD and PVD coated tools in machining of Incoloy 825. *Tribology International* Vol. 102, 2016, pp.198-212;
27. Trușculescu M, Ieremia A.: *Oțeluri inoxidabile și refractare*, Editura Facla, Timișoara, 1983;
28. *** Standard method of vibratory cavitation erosion test, ASTM, Standard G32, 2016;

